Functionalization of SBA-15 with APTES and Characterization of Functionalized Materials

A. S. Maria Chong and X. S. Zhao*

Department of Chemical and Environmental Engineering, National University of Singapore, Singapore 119260, Singapore

Received: June 30, 2003

The amine moiety is an important functionality for many applications such as enzyme immobilization on porous solid supports. In this study, mesoporous SBA-15 was functionalized by co-condensation of tetraethoxysilane (TEOS) with organosilane (aminopropyl)triethoxysilane (APTES) in a wide range of molar ratios of APTES:TEOS in the presence of triblock copolymer P123 under acidic synthetic conditions. The functionalized materials were characterized by physical adsorption, CHN elemental analysis, and various spectroscopic techniques. The data of FTIR, elemental analysis, XPS, and solid-state NMR demonstrated the incorporation of amine functional groups on the surface and inside the pore walls of the APTES-functionalized SBA-15 samples. The results of SAXS, N_2 adsorption, and TEM showed the effect of APTES present in the initial synthesis mixtures on the formation of SBA-15 mesostructure such as structural ordering, pore size, and surface area. Reasons behind the observed strong adverse effect of APTES on SBA-15 mesostructure were investigated.

Introduction

The advantages of immobilization of enzymes, cells, and antibodies onto solid supports were confirmed in 1916.[1] Since then, a great deal of research effort has been made at immobilization of enzymes to ease separation processes and to enable reuse of the immobilized enzymes, aimed at reducing the process cost.[2] In addition, immobilized enzymes have been observed to be more stable in a harsh reaction medium.[3,4]

Polymeric organic materials such as resins, organic gels, and fibers are the conventional support for the immobilization of enzymes. However, these materials have a low reusability, thus creating problems in disposal. On the other hand, inorganic supports such as porous silica gels are structurally more stable, environmentally more acceptable, and chemically more resistant to organic solvents and microbial attacks over the organic supports,[5−7] thus having been explored extensively. Of particular interest is the use of ordered mesoporous silica materials as a support for enzyme immobilization.[3,4,6−14] The controllable pore dimensions (20−500 Å), large specific surface area (∼1000 m^2/g), and highly ordered pore structure make themselves a very suitable support for immobilization of the enzymes. Among them, SBA-15, a mesoporous material synthesized by using triblock copolymer surfactant as a template under acidic conditions,[15] supersedes other mesoporous materials such as M41S because of its much larger pore size (up to 30 nm) and better stability. Larger pores enable immobilization of larger biomolecules, which cannot be accommodated in small pores.[3,8,11]

Surface modification using (3-aminopropyl)triethoxysilane (APTES), producing a terminal amine group ($-NH_2$), has been found to be useful for covalent coupling of protein to the surface of the silica materials.[16−20] In general, there are two approaches to surface modification, i.e., postmodification, also known as grafting, and direct synthesis or co-condensation.[21] Grafting is a method more commonly used in performing surface modification by covalently linking organosilane species with surface silanol groups (free and germinal silanol).[22] However, the grafting method has several shortcomings: (1) reduced pore size due to the attachment of a layer of functional moiety on the surface, leading to a less desirable product because the reduced pore size will cause a stronger diffusion resistance to protein molecules having a kinetic diameter of the similar size to the reduced pore size; (2) time-consuming as it needs two steps to accomplish the modification process; (3) limited accessible surface silanol groups on the mesoporous silica materials,[22] therefore only a low concentration of the organosilane can be attached; and (4) difficulties in controlling the loading and position of the organosilane.[23]

The co-condensation method was first reported by two research groups in 1996.[24,25] This method allows modification of the surfaces of the mesoporous materials in a single step by copolymerization of organosilane with silica or organosilica precursors in the presence of a surfactant.[24−37] This approach enables a higher and more homogeneous surface coverage of organosilane functionalities.[26] In addition, the stability of the postmodified materials is believed to be not as good as that of those materials prepared by co-condensation.[27]

A variety of functional groups have been incorporated into mesoporous materials such as aliphatic hydrocarbons,[23,24] thiol groups,[23,28−32] vinyl groups,[31,32] phenyl groups,[23,24,28,30,32,34] amine groups,[3,26,28−30,32,35] and perfluoro groups.[29,36,37] Most of these works have been conducted to modify M41S-designated materials under basic synthetic conditions.

Functionalization of SBA-15 with amine, thiol, nitrile, phenyl, and chloro groups has been studied by Yiu and co-workers for immobilization of trypsin enzyme.[3] The authors communicated the efficiency of the functionalized materials for enzyme immobilization whereas detailed characterization data were not presented. To the best of our knowledge, the synthesis chemistry, the influence of the molar ratio of organosilane to tetraethyl orthosilicate (TEOS) on the formation of SBA-15, and the

* To whom correspondence should be addressed: Tel (65) 68744727; Fax (65) 67791936; e-mail chezxs@nus.edu.sg.

10.1021/jp035877+ CCC: $25.00
Published on Web 10/24/2003

structural properties of the functionalized materials, etc., have not been fully explored.

This paper presents a study on the incorporation of amine group in SBA-15 via the co-condensation method. The effect of APTES on the formation of SBA-15 structure and detailed characterization results will be discussed in order to shed some light on the synthesis chemistry. The data of immobilization of penicillin amidase on the functionalized materials as well as enzymatic catalytic activity will be reported in a subsequent paper.

Experimental Part

Chemicals and Synthesis. Tetraethyl orthosilicate (TEOS, 98%, Acros Organics), surfactant poly(ethylene glycol)-*block*-poly(propylene glycol)-*block*-poly(ethylene glycol) (P123, Aldrich), (3-aminopropyl)triethoxysilane (APTES, 99%, Aldrich), 2 M hydrochloric acid prepared from 37% fuming hydrochloric acid (Merck), and absolute ethanol (99.98%, Merck) were used as received.

The preparation of a pure silica SBA-15 sample was similar to the method reported by Zhao et al.[15] 2 g of P123 was stirred with 15 mL of deionized water at 35 °C until fully dissolved, followed by adding 30 g of 2 M HCl solution and dropwise addition of 4.4 g of TEOS. The mixture was allowed to stir at 35 °C for 24 h before transferring into a Teflon bottle sealed in an autoclave, which was then heated to 100 °C for 2 days in an oven. The solid was filtered off, washed three times with deionized water, and calcined at 500 °C for 4 h.

The synthesis of APTES-functionalized SBA-15 materials was essentially similar to that of the pure-silica SBA-15, except for adding a certain amount of APTES. Samples synthesized with different ratios of APTES:TEOS are designated as 1:8APTES, 1:10APTES, 1:15APTES, and 1:20APTES (e.g., 1:8APTES represents the sample synthesized with a ratio of APTES:TEOS = 1:8). Removal of surfactant P123 was conducted by using ethanol extraction at 70 °C for 6 h, and this was repeated three times. The solid samples were filtered out, washed with ethanol, and dried at room temperature.

Characterization. Small-angle X-ray scattering (SAXS) measurements were performed on a NanoStar-Bruker instrument at 40 kV and 35 mA. The distance between sample and detector was 1.1 m. Cu Kα X-ray with a wavelength of $\lambda = 1.5418$ Å was used. N_2 adsorption measurements were performed on a NOVA 1000 system at liquid nitrogen temperature. Before measurement, about 0.4 g of sample was degassed at 120 °C for 3 h. The specific surface area of the samples were calculated by using the multiple-point Brunauer−Emmett−Teller (BET) method in the relative pressure range $P/P_0 = 0.05-0.3$. The pore size distribution curves were computed by using the Barrett−Joyner−Halenda (BJH) method, and pore sizes were obtained from the peak positions of the distribution curves. Transmission electron microscopy (TEM) was performed on a JEOL 2010 electron microscope, operated at an acceleration voltage of 200 kV. Thermogravimetric analysis (TGA) was performed on a TA Instrument TGA 2050 thermogravimetric analyzer with a heating speed of 20 °C/min under N_2 with a flow rate of 100 mL/min. Fourier transform infrared (FTIR) spectra were collected on a Bio-Rad FTS 135 with a resolution of 4 cm^{-1} by using the KBr method. X-ray photoelectron spectroscopy (XPS) measurements were conducted on a Kratos AXIS HSi spectrometer under a pressure below 5×10^{-8} Torr with a monochromatized Al Kα X-ray source (1486.6 eV photons) at constant dwelling time of 100 ms, a passing energy of 40 eV, and an anode current of 15 mA. C_{1s} of binding energy 284.6 eV was used as the reference. CHN elemental analyses were performed on a Perkin-Elmer series II CHNS/O analyzer 2400. A Perkin-Elmer microbalance of model AD-6 autobalance controller was used in weighing sample of around 1 mg. Purified air, oxygen, and helium were supplied to the combustion chamber at 60, 15, and 20 psi, respectively. Combustion temperature was set to 925 °C. The *K*-factor in the calibration of the analyzer using acetanilide revealed values of 16.5 ± 3.5 for carbon, 50 ± 20 for hydrogen, and 6.0 ± 3.0 for nitrogen. Organic analytical standard acetanilide (Perkin-Elmer, lot no. 121H0359) was used. Solid-state magic-angle spinning (MAS) nuclear magnetic resonance (NMR) spectra were obtained on a Bruker DRX400 MHz FT-NMR spectrometer with spectral widths of 30 303 and 40 323 Hz for ^{13}C and ^{29}Si, respectively. A 4 mm rotor was used. The MAS speed was 8 kHz. The cross-polarization (CP) technique was used for ^{13}C measurements while the single-pulse method was used for ^{29}Si spectrum collections. Both ^{13}C and ^{29}Si MAS NMR spectra were referenced to tetramethylsilane.

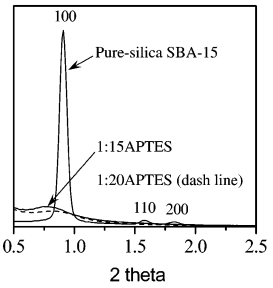

Figure 1. SAXS spectra of pure-silica SBA-15, 1:15APTES, and 1:20APTES.

Results and Discussion

Figure 1 compares the SAXS patterns of SBA-15 with 1:15APTES and 1:20APTES. Structural characterization of mesoporous silica materials by using SAXS has been explored recently.[38−41] The scattering vector *q* employed in SAXS analysis can be related to the diffraction angle (θ) by using the Bragg equation $\lambda = 2d \sin\theta$ with $q = 4\pi \sin\theta/\lambda$, where $\lambda = 1.5418$ Å. According to Figure 1, three well-resolved peaks can be observed on the pure-silica SBA-15 sample in the range of $2\theta = 0.9-2°$. The peaks can be indexed according to two-dimensional hexagonal *p6mm* symmetry, indicating a well-defined SBA-15 mesostructure.[15] However, only one very broad peak at 2θ ranging from 0.8 to 0.9 is seen on the functionalized SBA-15 samples. The much lower SAXS intensity and the disappearance of the peaks of 110 and 200 diffractions for samples 1:15APTES and 1:20APTES demonstrate a disordered mesostructure, indicating a strongly adverse effect of APTES on the formation of SBA-15. Such a strong effect was not observed under basic and neutral synthesis conditions,[26,28−30,32] indicating that the chemistry of acidic synthesis plays an important role in mesostructure formation, which will be further discussed below. SAXS measurement of samples 1:10APTES and 1:8APTES was not attempted because these two samples would be expected to display a featureless SAXS pattern.

The N_2 adsorption/desorption isotherms of the APTES-functionalized SBA-15 samples together with the pure-silica SBA-15 sample are shown in Figure 2. The BET surface area (S_{BET}) and total pore volume (V_{total}) are given in Table 1. The pure-silica SBA-15 sample displays a type IV isotherm with H1 hysteresis and a sharp increase in volume adsorbed at $P/P_0 \cong 0.76$, characteristic of highly ordered mesoporous materials. For samples 1:15APTES and 1:20APTES, they both

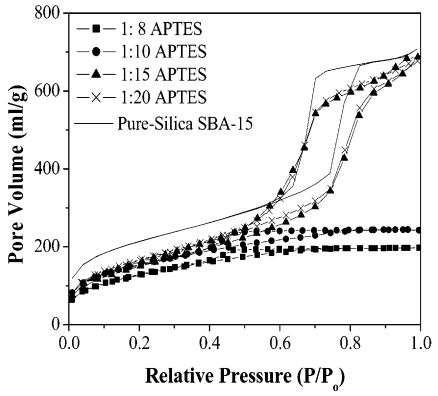

Figure 2. N_2 sorption isotherms of APTES-functionalized and pure-silica SBA-15 samples.

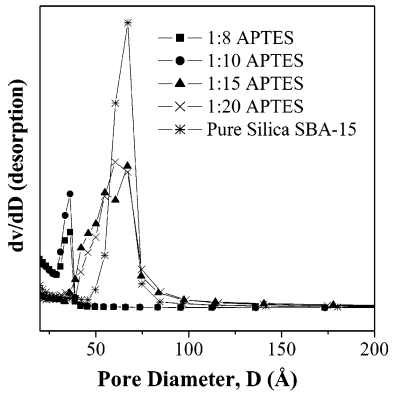

Figure 3. BJH pore size distribution curves of APTES-functionalized and pure-silica SBA-15 samples.

TABLE 1: Structural Properties of SBA-15 Samples Characterized by N_2 Adsorption

	D_{BJH} (Å)			
sample	adsorption	desorption	S_{BET} (m^2/g)	V_{total} (mL/g)
1:8APTES		36	466	0.31
1:10APTES		36	550	0.37
1:15APTES	90	67	550	1.0
1:20APTES	90	61	599	1.0
SBA-15	90	67	854	1.2

exhibit a type IV isotherm with a H1 hysteresis loop with a lower specific area and a slightly smaller pore volume in comparison with SBA-15. The pore size calculated from the adsorption branches is identical to that of SBA-15 silica. In addition, capillary condensation of N_2 occurred over a slightly wider P/P_0 range in these two APTES-functionalized samples than in the pure-silica SBA-15 sample. The above physisorption data indicate that, in the presence of a relatively low concentration of APTES, the textural properties of SBA-15 were substantially maintained despite significant structural disordering as revealed by the SAXS data in Figure 1. For samples 1:8APTES and 1:10APTES, the isotherms are of type I without observation of sharp increase in volume adsorbed because of capillary condensation, indicating a microporous material. A very small hysteresis loop of H2 type, as classified in IUPAC manual, can be seen. This kind of hysteresis loop is commonly found in some materials that are structurally disordered with a broad distribution of pore size and an ill-defined pore shape.[42] The nitrogen adsorption data indicate that the amount of APTES present during synthesis in the co-condensation method has a profound effect on the formation of SBA-15 mesostructure.

Shown in Figure 3 are the BJH pore size distribution curves computed from the desorption isotherms of the various SBA-15 samples. The pore sizes (D_{BJH}) estimated from the peak positions of the BJH pore size distribution curves measured from both the adsorption and desorption isotherms are included in Table 1. It is seen that both 1:15APTES and 1:20APTES samples possess a similar pore size to that of the pure-silica SBA-15 sample but with a slightly broader distribution and a lower intensity, indicating a less ordered pore structure. In the presence of relatively large amount of APTES in the initial synthesis mixture (samples 1:10APTES and 1:8APTES), the pore size became 36 Å calculated from the desorption branches. Such a significant decrease in pore diameter indicates the presence of micropores. Nevertheless, the two samples synthesized with APTES:TEOS $\leq$ 15 possess a much better ordered structure than the two samples synthesized with APTES:TEOS $\geq$ 10. This indicates that there is an optimum range of molar ratio of APTES:TEOS that can be employed to synthesize

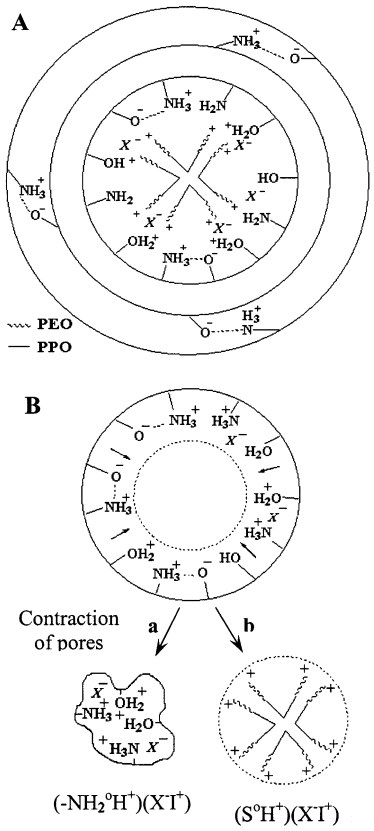

Figure 4. (A) An illustration of local structure disordering of silicate walls because of cross-linking of protonated amines with silanols and the weaker interactions between P123 and silicate species because of zwitterions. (B) A scheme showing pore contraction because of the presence of protonated amine groups (a) in comparison with the absence of organosilane APTES. I = silicate precursor; S^0 = neutral surfactant; X^- = mediated counterions.

functionalized SBA-15 with a high loading of functionality yet a good mesostructure. The uniformity of pore size greatly depends on the molar ratio of APTES:TEOS used in synthesis.

The loading of aminopropyl groups achievable without significant loss of structure under neutral[26,35] and basic[9,30,32] synthesis conditions is much higher than for the present acidic route. The stronger adverse effect of APTES on the formation of mesostructure under acidic synthesis conditions than under basic or neutral conditions is believed to be related to the following aspects. First, as illustrated in Figure 4A, amine groups of APTES are known to be easily protonated under acidic conditions;[43,44] such protonated amine groups would have cross-linked with silanol groups of the silicate species, resulting in

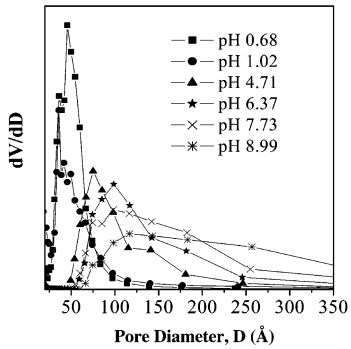

Figure 5. BJH pore size distribution curves (from desorption isotherms) of various 1:15APTES samples synthesized at different pH values.

local disruptions of the silicate walls as reflected by the SAXS patterns with only one very broad peak. On the other hand, as suggested by Walcarius and co-workers,[44] protonated terminal amine groups can interact with silanol groups to form zwitterions ($-NH_3^+ - - - ^-OSi$). The formation of such zwitterions on the pore surface would have prevented direct interactions of surfactant P123 with the silicates, leading to a less ordered pore structure. Second, it is known that the formation of mesoporous SBA-15 silica under acidic conditions is via a mechanism of $(S^0H^+)(X^-I^+)$.[15,45] In the presence of APTES in the synthesis system, we believe that competitive interactions have taken place as illustrated in Figure 4B. Those silicate species connected with APTES having protonated amine groups ($-NH_2H^+$) would have competed with those positively charged silicate species ($SiOH_2^+$) for surfactant P123 to form $(-NH_2H^+)(X^-SiOH_2^+)$, leading to microporosity as revealed by the nitrogen adsorption data. Third, the interactions of the amine groups with the hydrophilic EO moieties were disrupted by a contrast matching of the surfactant headgroup with the organosilane.[23,46] The long-chain aminopropyl groups with a hydrophilic tail of protonated amine groups directing toward the micelle cores caused a repulsion as the micelle cores are composed of hydrophobic PPO blocks.[15] Fourth, because APTES is basic in nature, an increase in the percentage of APTES added to the synthesis medium resulted in pH increase. It was observed that the pH increased from −0.25 to 0.33 as the amount of APTES was increased from 5 to 17%, resulting in structure disordering as has been observed by Choi and co-workers on SBA-15 silicas.[47] To clarify this point, the pH was varied from 1.02 to 8.99 during the synthesis of a series of 1:15APTES samples. The BJH pore size distribution curves shown in Figure 5 clearly show that as the pH was increased the pore size distribution curves became broader and broader while the pore sizes increased gradually, indicating the effect on pH of the synthesis system on the pore structures. As suggested previously,[47] the condensation rate of silica precursor becomes faster than its hydrolysis rate as pH is increased, leading to incomplete hydrolysis of the silica precursor.

The data in Table 1 also shows that the BJH pore diameters of samples 1:15 APTES, 1:20APTES, and pure-silica SBA-15 measured from the adsorption isotherms (of about 90 Å) are all larger than that measured from the desorption isotherms (of around 60−70 Å). There is a difference of about 20 Å. The underestimation of pore size of the BJH model based on desorption isotherm has already been recognized,[48] and the adsorption isotherm has been recommended for evaluation of mesopore size.[49] This conclusion can be supported by the TEM data presented below.

The TEM images of the pure-silica SBA-15 and 1:20APTES samples are compared in Figure 6. The hexagonally arranged

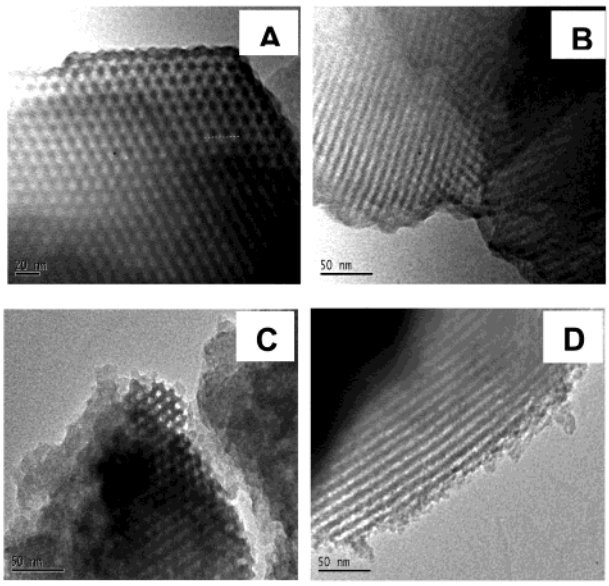

Figure 6. TEM images of pure-silica SBA-15 (A and B) and sample 1:20APTES (C and D) viewed from perpendicular direction (A and C) and parallel direction (B and D).

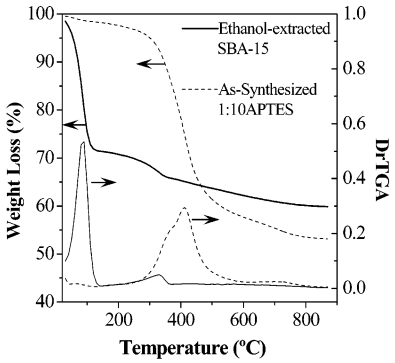

Figure 7. TGA and DrTGA curves of as-synthesized SBA-15 and solvent-extracted 1:10APTES.

pore arrays of the pure-silica SBA-15 sample can be clearly seen, which was disrupted by the incorporation of APTES functionality. The pore diameter of the pure-silica SBA-15 sample estimated from the TEM image is around 90 Å, which is in good agreement with that estimated from the BJH adsorption isotherm, supporting the work of Kruk and co-workers.[49]

Figure 7 shows the weight loss (TGA) and derivative weight loss (DrTGA) curves of sample 1:10APTES before (dash lines) and after solvent extraction (solid lines). For the as-synthesized sample, one major weight loss (about 35.4%) event in the temperature range of 300−500 °C is seen. This is mainly due to the thermal removal of surfactant P123.[15,45] Decomposition of APTES could have also happened in this temperature range. A small peak at about 700 °C can be seen as well. This is likely due to the dehydroxylation of the silicate networks as observed on mesoporous pure-silica materials[50] and/or the elimination of residual ethoxy groups because of incomplete hydrolysis of TEOS. Two peaks can be seen from the DrTGA curve of the ethanol-extracted sample. The one observed at about 90 °C is due to physically adsorbed water while the other one at about 320 °C could be due to the thermal decomposition of protonated amines and/or incompletely removed surfactant.

The incorporation of amine groups in the silicate frameworks can be qualitatively confirmed by the FTIR data shown in Figure 8. At 673 cm^{-1}, a weak peak is seen on sample 1:20APTES,

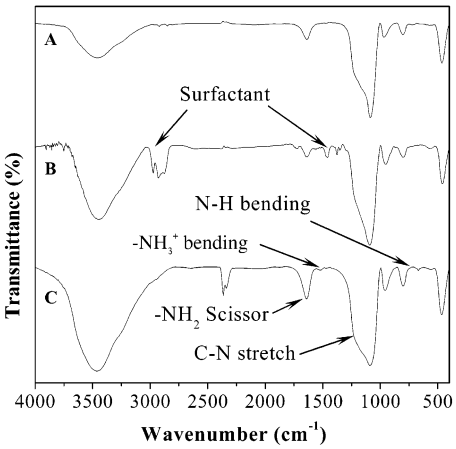

Figure 8. FTIR spectra of (A) calcined SBA-15, (B) as-synthesized SBA-15, and (C) ethanol-extracted 1:20 APTES.

TABLE 2: ESCA and Elemental Analysis Data of APTES-Functionalized SBA-15 Samples[a]

sample	element content (wt %)				amine density[b]
	C	N	O	Si	
1:8 APTES	27.69 (6.18)	1.65 (2.61)	46.34	24.33	1.18 (1.9)
1:10 APTES	23.38 (5.50)	1.58 (1.38)	49.45	25.59	1.13 (1.0)
1:15 APTES	16.04 (4.62)	1.43 (1.09)	53.86	28.67	1.02 (0.8)
1:20 APTES	16.73 (3.14)	1.43 (0.94)	53.02	28.82	1.02 (0.7)

[a] Values in parentheses were obtained from CHN elemental analysis. [b] In mmol of NH_2/g.

which is due to the bending of N−H bonds, and the symmetrical $-NH_3^+$ bending at 1510 cm^{-1}, indicating the existence of amine groups. The C−N stretching vibration is normally observed in the wavenumber range 1000−1200 cm^{-1}.[51] However, this peak was not resolved due to the overlay with the IR absorptions of Si−O−Si in the range 1130−1000 cm^{-1} and of $Si-CH_2-R$ in the range 1250−1200 cm^{-1}.[43] Nevertheless, the peak in this region for the APTES-modified SBA-15 sample is broader, indicating possible overlap of peaks. In addition, the peak at 1650 cm^{-1}, which can be assigned to N−H bending, is very intensive for the APTES-modified sample, indicating the presence of N−H groups. A pure-silica SBA-15 was reported to have three strong peaks in this region at about 3747, 3680, and 3535 cm^{-1}.[43,52] The peak at 3747 cm^{-1} is due to silanol groups while the other two peaks are due to adsorbed or hydrogen-bonded water molecule.[52] The material itself was extremely hygroscopic; therefore, the significant peaks were covered by a broad −OH peak. The width of this broad peak at 3500 cm^{-1} for APTES-functionalized sample slightly increased. This widening of the peak may be due to the symmetric stretching of N−H. The N−H stretching was reported around 3346 cm^{-1} for free amine and around 3305 cm^{-1} for terminal amine groups, respectively, which are cross-linked with the silanol group.[43]

Table 2 lists the chemical compositions of the APTES-functionalized samples analyzed by using both ESCA and CHN element analysis (in parentheses) for the APTES-functionalized samples. It is seen that reasonable amounts of both carbon (C) and nitrogen (N) were detected in the samples. The increment of C and N is proportional to the amount of APTES added during synthesis. The experimental weight ratio of C:N was found to be slightly larger than the theoretical value for all samples. This could be due to those carbons from ethoxy groups because of incomplete hydrolysis of TEOS and/or from surfactant P123 that was not removed during solvent extraction. While elemental analysis measures the bulk quantity of a substance, XPS measures the surface composition of a depth of about 10 nm. From Table 2 it is also seen that the mass concentration of N of sample 1:20 APTES was measured to be 1.43%, which is about 34% more than that measured by elemental analysis. However, at a higher APTES concentration, the nitrogen contents measured by XPS are lower than that measured by CHN. Nevertheless, the N contents measured by XPS are fairly in good agreement with those measured by elemental analysis, showing that amine functional groups are relatively uniformly distributed on the pore surface and in the pore walls. The observed much higher C content for all samples analyzed by XPS than that analyzed by elemental analysis is most likely due to the presence of residual surfactant P123 on the pore surface.

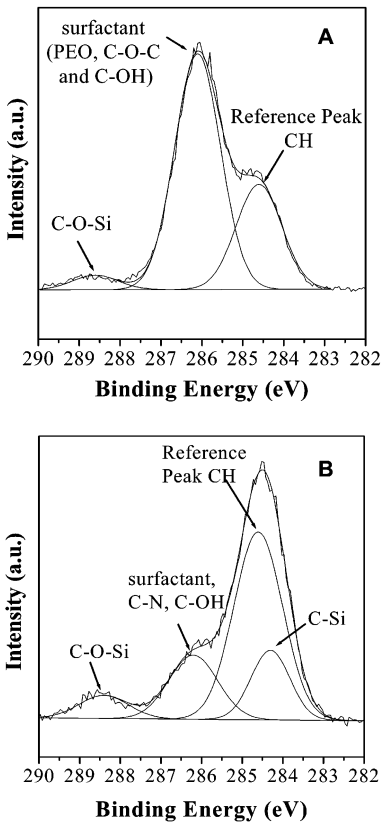

Figure 9. C_{1s} XPS spectra of (A) SBA-15 and (B) 1:20APTES before template removal.

Shown in Figure 9 are the C_{1s} spectra of as-synthesized pure-silica SBA-15 (A) and sample 1:20APTES (B). The peak areas together with other APTES-functionalized SBA-15 materials are compiled in Table 3. The peaks that are observed on the pure-silica SBA-15 sample at 284.6 and 286.1 eV can be assigned to C−H, C−OH, and C−O in $(-CH_2CH_2O-)_n$ moieties, respectively.[53−55] However, the appearance of a small peak at 288.6 eV, which is assigned to C−O−Si species,[56] was not expected. The presence of C−O−Si species is most probably due to incomplete hydrolysis of TEOS as has been commented by Yoshitake et al.[57]

The three peaks observed on the as-synthesized pure-silica SBA-15 sample can also be seen on sample 1:20APTES, but with different intensities. The most intensive peak of sample 1:20APTES is observed at 284.6 eV, attributed to C−H in APTES. The intensity of this peak observed on sample 1:20APTES is much stronger than that observed on the pure-silica SBA-15 sample. In addition to the three peaks, one more peak at 284.3 eV, which is attributed to C−Si due to −Si−

TABLE 3: Peak Area of Chemical Species C−H, C−Si, C−N, C−O−Si, C−NH_2, and NH_3^+ Obtained from Curve Fitting of XPS Spectra

sample	C−H	C−Si	C−N + C−OH	C−O−Si	C−NH_2	−NH_3^+
1:8 APTES	1924	1130	698	284	408	896
1:10 APTES	3664	1096	1597	388	911	1008
1:15 APTES	1347	1088	1249	162	368	519
1:20 APTES	1495	438	510	183	452	427

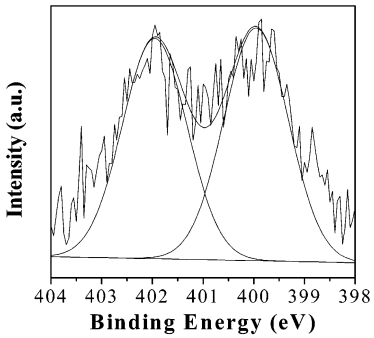

Figure 10. N_{1s} XPS spectra of 1:20APTES: C−NH_2 (399.9 eV) and NH_3^+ (401.9 eV).

$(CH_2)_3$−NH_2 in APTES, is also seen. The peak at about 286.2 eV for sample 1:20APTES, which is the most intensive peak for the as-synthesized pure-silica SBA-15 sample (it was 286.1 eV), can be assigned to two species: one is C−OH,[54] while the other is C−N due to APTES.[55] The former species may be due to ethanol that was used during template removal. The data of curve fitting in Table 3 show that the C−Si peak areas of samples 1:10APTES, 1:15APTES, and 1:20APTES are all smaller than that of the C−N peak, while in APTES the ratio of these two chemical species is 1:1. This indicates the possibility of residue ethanol. As for sample 1:8APTES, the peak area of C−Si is larger than that of C−N, which might be due to the protonation of terminal amine groups, reducing C−N species. It is likely that the high concentration of organosilane promotes the reaction of terminal amine group with silanol groups of the silica precursor.[43]

The presence of protonated amine groups is evident from the N_{1s} spectra shown in Figure 10. Two peaks with a binding energy region 399.9 and 401.9 eV and a ratio of peak area is of almost 1:1 are seen. The standard binding energy for the free amine group (−NH_2) falls in the region of 399−401 eV, while the protonated amine (−NH_3^+) has a higher binding energy of 1.5 eV above the free amine.[58] Thus, the peak at 399.9 eV is assigned to the −NH_2 while the peak at 401.9 eV is attributed to protonated amine groups.

The incorporation of APTES can be further justified by the XPS spectra of N_{1s}, as shown in Figure 11. No peak in the range 396−402 eV is seen on the pure-silica SBA-15 sample, but peaks are seen on all APTES-functionalized SBA-15 samples. The previous assignment of the peak at 286.2 eV due to C−N is justified here.

Figure 12 shows the solid-state ^{13}C CP-MAS NMR spectra of pure-silica SBA-15 before and after calcination, together with solvent-extracted 1:10APTES. In addition to the peaks attributed to surfactant P123 that are observed on the as-synthesized SBA-15 sample while not seen on the calcined sample, the APTES-functionalized SBA-15 sample exhibits extra resonance peaks at chemical shifts $\delta = 8$, 20, and 41 ppm, respectively. These peaks were attributed to different carbon environments in the organosilane as denoted as C^1, C^2, and C^3,[11,29] showing the incorporation of amine functional groups. The observation of

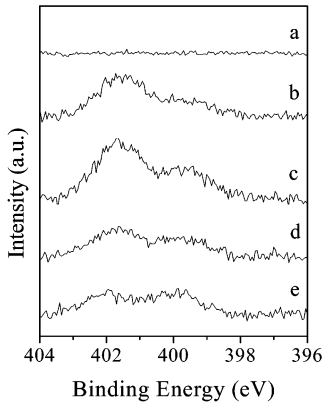

Figure 11. N_{1s} XPS spectra of (a) SBA-15, (b) 1:8APTES, (c) 1:10APTES, (d) 1:15APTES, and (e) 1:20APTES after template removal.

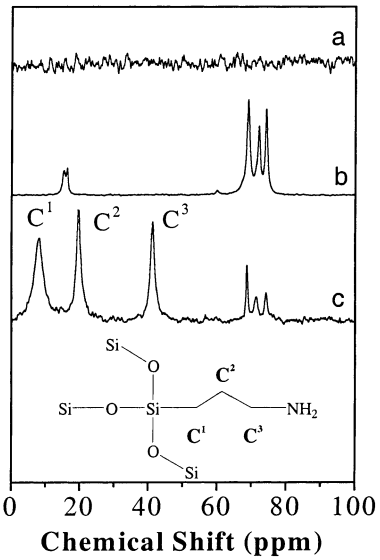

Figure 12. ^{13}C CP-MAS NMR spectra of (a) calcined SBA-15, (b) as-synthesized SBA-15, and (c) solvent-extracted 1:10APTES.

resonance peaks in the range of $\delta = 67-77$ ppm and a small peak at about 15 ppm on sample 1:10APTES confirms the incompleteness of surfactant removal by solvent extraction. Nevertheless, the intensities of the peaks due to P123 are relatively weaker than that of those due to amine functionality, showing that the leftover of surfactant P123 is not much.

Figure 13 depicts the ^{29}Si CP-MAS NMR spectra of pure-silica SBA-15 and APTES-functionalized SBA-15 samples. Three resonance peaks because of the Si environments of Q^4 ($\delta = -110$ ppm), Q^3 ($\delta = -102$ ppm), and Q^2 ($\delta = -92$ ppm) can be seen.[22,59,60] In addition to these three peaks, samples 1:10APTES and 1:20APTES display two more resonance peaks at $\delta = -65$ ppm, assigned to T^3, and at −57 ppm, attributed to T^2. These two peaks are due to the Si atoms of different environments in the organosilane APTES. It is seen that sample 1:10APTES possesses a higher intensity of both T sites than sample 1:20APTES, demonstrating a higher content of amine groups of the former than the latter. It can also be seen that the

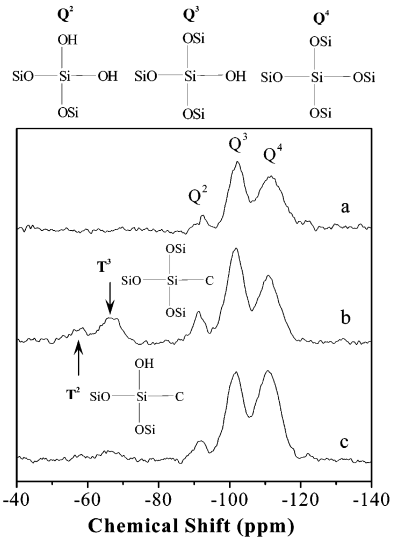

Figure 13. ^{29}Si CP-MAS NMR spectra of (a) SBA-15, (b) 1:10APTES, and (c) 1:20APTES.

ratio of the peak intensity of Q^4:Q^3 for sample 1:20APTES is higher than that for sample 1:10APTES, showing a higher condensation of the silicate network of sample 1:20APTES than that of sample 1:10APTES. This indicates the strongly disruptive effect of APTES on the local structures of the silicate framework under the experimental conditions.

Conclusions

Functionalization of mesoporous SBA-15 via co-condensation of tetraethoxysilane with aminopropylsilane under a strong acidic condition is an easier and more controllable method than grafting. The co-condensation method enables a better control of the pore size and the density of functional groups. Highly ordered hexagonal pore structures with uniform pore size of about 90 Å, almost the same as pure-silica SBA-15 materials, can be obtained when the molar ratio of APTES:TEOS is in a reasonable range (e.g., samples 1:15APTES and 1:20APTES). The mesostructures of APTES-functionalized SBA-15 materials prepared with a molar ratio of APTES:TEOS lower than 15 can be substantially conserved. This has to be compensated by a lower density of the functional groups. A molar ratio of APTES:TEOS beyond the range yields mesostructures with fairly high surface area and pore volume but without long-range ordering. Under acidic synthesis conditions, aminopropylsilane has a profound effect on both the local structures of the silicate framework and the pore structure of SBA-15 because of the protonation of amine groups. Such a strong adverse effect has not been observed under basic synthesis conditions.

Acknowledgment. We thank ARF of NUS and A*STAR for financial support. We also thank Dr. Li Jun and Dr. Li Xu for measurement of SAXS spectra. Dr. Yang Daiwen and Ms. Han Yanhui at the Department of Chemistry and Biological Sciences, National University of Singapore, are acknowledged for their help on NMR measurements. A.S.M.C. thanks Dr. Guo Wanping for valuable discussions.

References and Notes

(1) Pope, N. M.; Kulcinski, D. L.; Hardwick, A.; Chang, Y. A. *Bioconjugate Chem.* **1993**, *4*, 166−171.
(2) Tischer, W.; Kasche, V. *TIBTECH* **1999**, *17*, 326−335.
(3) Yiu, H. H. P.; Botting, C. H.; Botting, N. P.; Wright, P. A. *Phys. Chem. Chem. Phys.* **2001**, *3*, 2983−2985.
(4) He, J.; Li, X.; Evans, D. G.; Duan, X.; Li, C. *J. Mol. Catal. B: Enzym.* **2000**, *11*, 45−53.
(5) Maladkar, N. K. *Industrial Biotechnology*; International Science Publisher: New York, 1991.
(6) Deere, J.; Magner, E.; Wall, J. G.; Hodnett, B. K. *Chem. Commun.* **2001**, 465−466.
(7) Deere, J.; Magner, E.; Wall, J. G.; Hodnett, B. K. *J. Phys. Chem. B* **2002**, *106*, 7340−7347.
(8) Takahashi, H.; Li, B.; Sasaki, T.; Miyazaki, C.; Kajino, T.; Inagaki, S. *Chem. Mater.* **2000**, *12*, 3301−3305.
(9) Yiu, H. H. P.; Wright, P. A.; Botting, N. P. *Microporous Mesoporous Mater.* **2001**, *44*−*45*, 763−768.
(10) Washmon-Kriel, L.; Jimenez, V. L.; Balkus Jr., K. J. *J. Mol. Catal. B: Enzym.* **2000**, *10*, 453−469.
(11) Yiu, H. H. P.; Wright, P. A.; Botting, N. P. *J. Mol. Catal. B: Enzym.* **2001**, *15*, 81−92.
(12) Takahashi, H.; Li, B.; Sasaki, T.; Miyazaki, C.; Kajino, T.; Inagaki, S. *Microporous Mesoporous Mater.* **2001**, *44*−*45*, 755−762.
(13) Lei, C.; Shin, Y.; Liu, J.; Ackerman, E. J. *J. Am. Chem. Soc.* **2002**, *124*, 11242−11243.
(14) Kisler, J. M.; Stevens, G. W.; O'Connor, A. J. *Mater. Phys. Mech.* **2001**, *4*, 89−93.
(15) Zhao, D.; Huo, Q.; Feng, J.; Chmelka, B. F.; Stucky, G. D. *J. Am. Chem. Soc.* **1998**, *120*, 6024−6036.
(16) Gass, T.; Ligler, F. S. *Immobilized Biomolecules in Analysis*—*A Practical Approach*; Oxford University Press: New York, 1998.
(17) Woodward, J., Ed.; *Immobilized Cells & Enzymes: A Practical Approach*; Oxford: England, 1985.
(18) Subramanian, A.; Kennel, S. J.; Oden, P. I. *Enzyme Microb. Technol.* **1999**, *24*, 26−34.
(19) Taylor, R. F., Ed.; *Protein Immobilization: Fundamentals and Applications*; Marcel Dekker: New York, 1991.
(20) Tisher, W.; Wedekind, F. *Topics in Current Chemistry*—*Immobilized Enzymes: Method and Applications;* Springer-Verlag: Berlin, 1999; Vol. 200.
(21) Stein, A.; Melde, B. J.; Schroden, R. C. *Adv. Mater.* **2000**, *12*, 1403−1419.
(22) Zhao, X. S.; Lu, G. Q. *J. Phys. Chem. B* **1998**, *102*, 1556−1561.
(23) Mercier, L.; Pinnavaia, T. J. *Chem. Mater.* **2000**, *12*, 188−196.
(24) Burkett, S. L.; Sims, S. D.; Mann, S. *Chem. Commun.* **1996**, 1367−1368.
(25) Macquaire, J. D. *J. Chem. Soc., Chem. Commun.* **1996**, 1961−1962.
(26) Richer, R.; Mercier, L. *Chem. Commun.* **1998**, 1775−1776.
(27) Macquaire, J. D.; Jackson, D. B.; Mdoe, J. E. G.; Clark, J. H. *New J. Chem.* **1999**, *23*, 539−544.
(28) Hall, S. R.; Davis, S. A.; Mann, S. *Langmuir* **2000**, *16*, 1454−1456.
(29) Fowler, C. E.; Burkett, S. L.; Mann, S. *Chem. Commun.* **1997**, 1769−1770.
(30) Hall, S. R.; Fowler, C. E.; Lebeau, B.; Mann, S. *Chem. Commun.* **1999**, 201−202.
(31) Babonneau, F.; Leite, L.; Fontlupt, S. *J. Mater. Chem.* **1999**, *9*, 175−178.
(32) Burleigh, M. C.; Markowitz, M. A.; Spector, M. S.; Gaber, B. P. *J. Phys. Chem. B* **2001**, *105*, 9935−9942.
(33) Lim, M. H.; Stein, A. *Chem. Mater.* **1999**, *11*, 3285−3295.
(34) Bambrough, C. M.; Slade, R. C. T.; Williams, R. T. *J. Mater. Chem.* **1998**, *8*, 569−571.
(35) Macquarrie, D. J. *Green Chem.* **1999**, 195−198.
(36) Corriu, R. J. P.; Mehdi, A.; Reyé, C. *C. R. Acad. Sci., Ser. II C* **1999**, *2*, 35−39.
(37) Corriu, R. J. P.; Datas, L.; Guari, Y.; Mehdi, A.; Reyé, C.; Thieuleux, C. *Chem. Commun.* **2001**, 763−764.
(38) Cho, Y. S.; Park, J. C.; Lee, B.; Kim, Y.; Yi, J. *Catal. Lett.* **2002**, *81*, 89−96.
(39) Jang, J.; Lim, B.; Lee, J.; Hyeon, T. *Chem. Commun.* **2001**, 83−84.
(40) Li, Z. H.; Gong, Y. J.; Wu, D.; Sun, Y. H.; Wang, J.; Liu, Y.; Dong, B. Z. *Surf. Interface Anal.* **2001**, *31*, 897−900.
(41) Sassi, Z.; Bureau, J. C.; Bakkali, A. *Vib. Spectrosc.* **2002**, *28*, 251−262.
(42) Gregg, S. J.; Sing, K. S. W. *Adsorption, Surface Area and Porosity*, 2nd ed.; Academic Press: London, 1982.
(43) White, L. D.; Tripp, C. P. *J. Colloid Interface Sci.* **2000**, *232*, 400−407.
(44) Walcarius, A.; Etienne, M.; Lebeau, B. *Chem. Mater.* **2003**, *15*, 2161−2173.
(45) Zhao, D.; Feng, J.; Huo, Q.; Melosh, N.; Fredrickson, G. H.; Chmelka, B. F.; Stucky, G. D. *Science* **1998**, *279*, 548−552.
(46) Melero, J. A.; Stucky, G. D.; Grieken, R.; Morales, G. *J. Mater. Chem.* **2002**, *12*, 1664−1670.

(47) Choi, D.; Yang, S. J. *J. Colloid Interface Sci.* **2003**, *261*, 127−132.
(48) Zhu, H.; Zhao, X. S.; Lu, G. Q.; Do, D. D. *Langmuir* **1996**, *12*, 6513−6517.
(49) Kruk, M.; Jaroniec, M.; Sayari, A. *J. Phys. Chem. B* **1997,** *101*, 583−589.
(50) Zhao, X. S.; Lu, G. Q.; Whittaker, A. K.; Millar, G. J.; Zhu, H. Y. *J. Phys. Chem. B* **1997,** *101*, 6525−6531.
(51) Shriner, R. L.; Hermann, C. K. F.; Morril, T. C.; Curtin, D. Y.; Fuson, R. C. *The Systematic Identification of Organic Compounds*, 7th ed.; John Wiley & Sons: New York, 1998.
(52) Scott, R. P. W. *Silica Gel & Bonded Phases, Their Production, Properties & Use in LC;* Wiley Science: New York, 1993.
(53) Moulder, J. F., Stickle, W. F., Sobol, P. E., Bomben, K. D., Chastian, J., Eds.; *Handbook of X-ray Photoelectron Spectroscopy a Reference Book of Standard Spectra for Identification & Interpretation of XPS Data*; Perkin-Elmer Corp. Physical Electronics Division: Eden Prairie, MN, 1992.
(54) Matuana, L. M.; Balatinecz, J. J.; Park, C. B.; Sodhi, R. N. S. *Wood Sci. Technol.* **1999**, *33*, 259−270.
(55) Niimura, N.; Miyakoshi, T. *Surf. Interface Anal.* **2000**, *29*, 381−385.
(56) Hijikata, Y.; Yaguchi, H.; Yoshikawa, M.; Yoshida, S. *Mater. Sci. Forum* **2002**, *389*−*393*, 1033−1036.
(57) Yoshitake, H.; Yokoi, T.; Tatsumi, T. *Chem. Mater.* **2002,** *14*, 4603−4610.
(58) http://www.geocities.com/capecanaveral/6737/esca1.html.
(59) Igarashi, N.; Hashimoto, K.; Tatsumi, T. *J. Mater. Chem.* **2002**, *12*, 3631−3636.
(60) Juan, F.; Ruiz-Hitzky, E. *Adv. Mater.* **2000**, *12*, 430−432.